Silver(I) complexes with *N*-methylphenothiazine as potential antimicrobial agents with a multi-target mode of action

Tina P. Andrejević,[a] Jovica Branković,[a] Tatjana Ilic-Tomic,[b] Nevena Stevanović,[a] Bojana Pantović,[a] Darko P. Ašanin,[c] Jasmina Nikodinovic-Runic,[b] Vladimir P. Petrović,[a] Violeta R. Marković,[a*] and Biljana Đ. Glišić[a*]

[a] *University of Kragujevac, Faculty of Science, Department of Chemistry, R. Domanovića 12, 34000 Kragujevac, Serbia*

[b] *Institute of Molecular Genetics and Genetic Engineering, University of Belgrade, Vojvode Stepe 444a, 11042 Belgrade, Serbia*

[c] *University of Kragujevac, Institute for Information Technologies Kragujevac, Department of Natural Sciences, Liceja Kneževine Srbije 1A, 34 000 Kragujevac, Serbia*

[*]Corresponding authors.

E-mail addresses: violeta.markovic@pmf.kg.ac.rs (V.R. Marković); biljana.glisic@pmf.kg.ac.rs (B.Đ. Glišić).

Abstract

N-Methylphenothiazine (*N*-Mephtz) was used as a ligand for the synthesis of three new silver(I) complexes with the general formula $[Ag(N\text{-Mephtz})_4]X\cdot nH_2O$ (X is $CF_3SO_3^-$ and n = 1/3 for **1**, X is SbF_6^- and n = 0 for **2**, and X is PF_6^- and n = 0 for **3**). These complexes were characterized using spectroscopic methods, while their structures were determined by single crystal X-ray diffraction analysis. In all complexes, four *N*-Mephtz ligands are monodentately coordinated to the silver(I) ion through the sulfur atom, forming cationic $[Ag(N\text{-Mephtz})_4]^+$ species, with $CF_3SO_3^-$, SbF_6^- and PF_6^- acting as counterions for **1**–**3**, respectively. Experimental IR band assignments were supported by DFT calculations, and TD-DFT simulations provided insight into their UV-Vis spectra. The antimicrobial activity of complexes **1**–**3** was evaluated against different bacterial and one fungal strain, with complex **1** exhibiting notable activity against all tested microorganisms, with MIC values ranging from 8 to 30 μg mL^{-1} (7.17 to 26.88 μM). Molecular docking screening identified eight potential antimicrobial protein targets among tested microorganisms. Cytotoxicity assessments revealed pronounced effects on human lung cancer (A549) and colon cancer (HCT116) cell lines, suggesting potential antiproliferative activity. However, the observed cytotoxicity toward mammalian cells also indicates the need for further structural refinement to improve selectivity for antimicrobial applications. The interactions of the complexes with calf thymus DNA (ct-DNA) and bovine serum albumin (BSA) were examined to assess their biomolecular binding affinities. The binding constant (K_A) indicated that complexes **1** and **3** have a similar binding affinity to this protein as *N*-Mephtz, while complex **2** demonstrated a lower affinity. All complexes exhibited significantly enhanced ct-DNA binding *via* the minor groove compared to the free ligand. Molecular docking confirmed strong minor groove DNA interactions and identified favorable BSA binding sites.

Keywords: Silver(I) complexes; Phenothiazine; Antimicrobials; DNA/BSA interactions; Molecular docking

TABLE OF CONTENTS

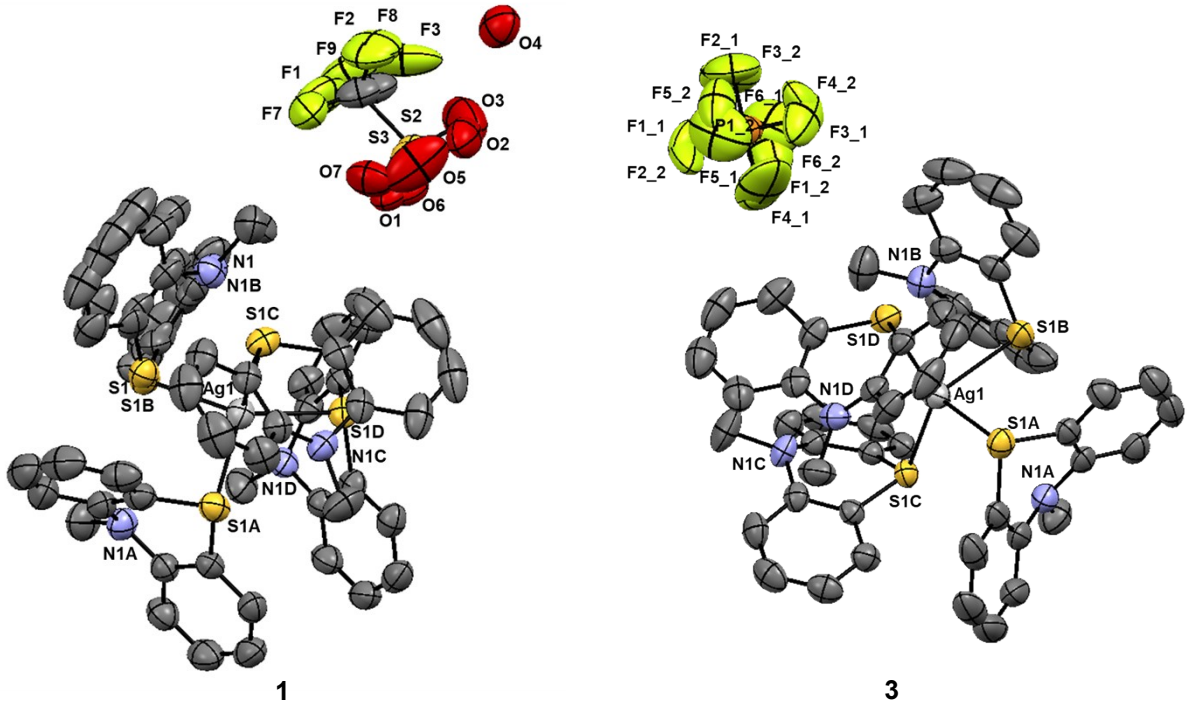

Fig. S1 Molecular structures of silver(I) complexes **1** and **3**. Hydrogen atoms are omitted for clarity. Displacement ellipsoids are drawn at 50% probability level.

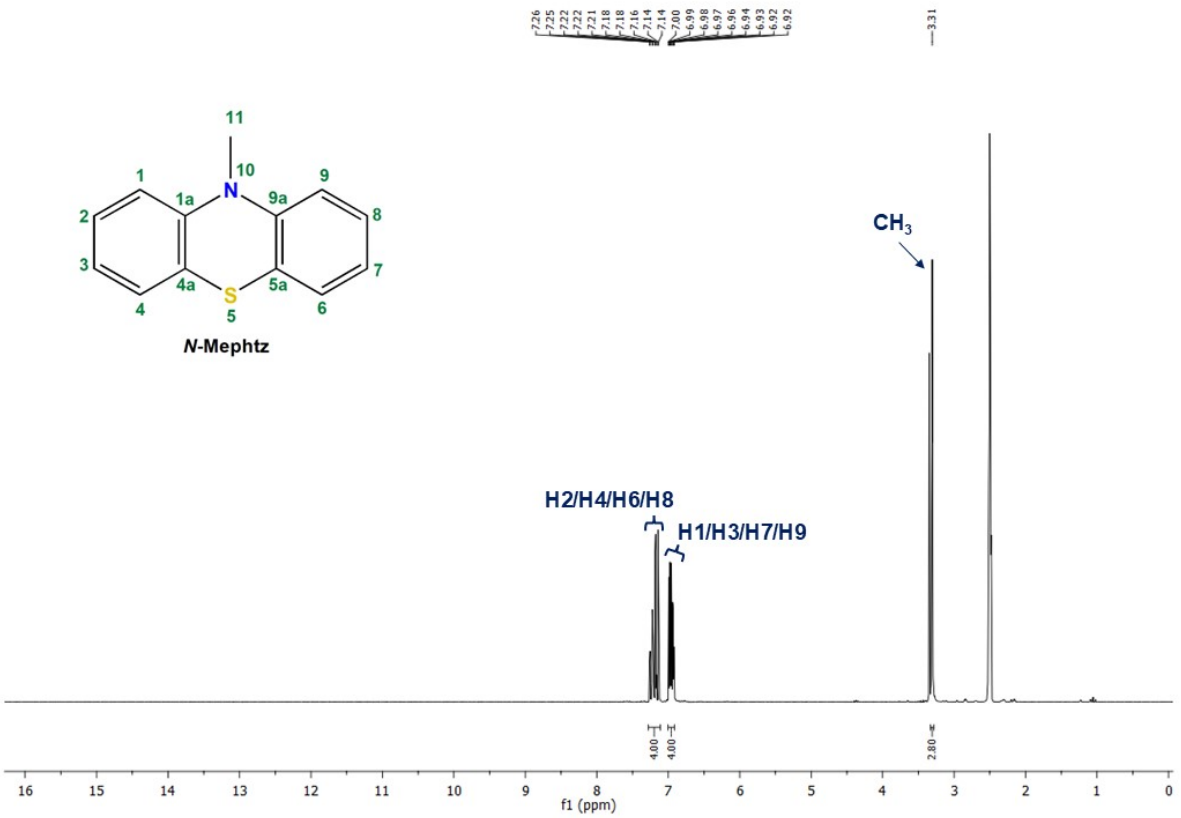

Fig. S2 ^{1}H NMR spectrum of *N*-Mephtz with atom numeration (DMSO-d_6, 200 MHz).

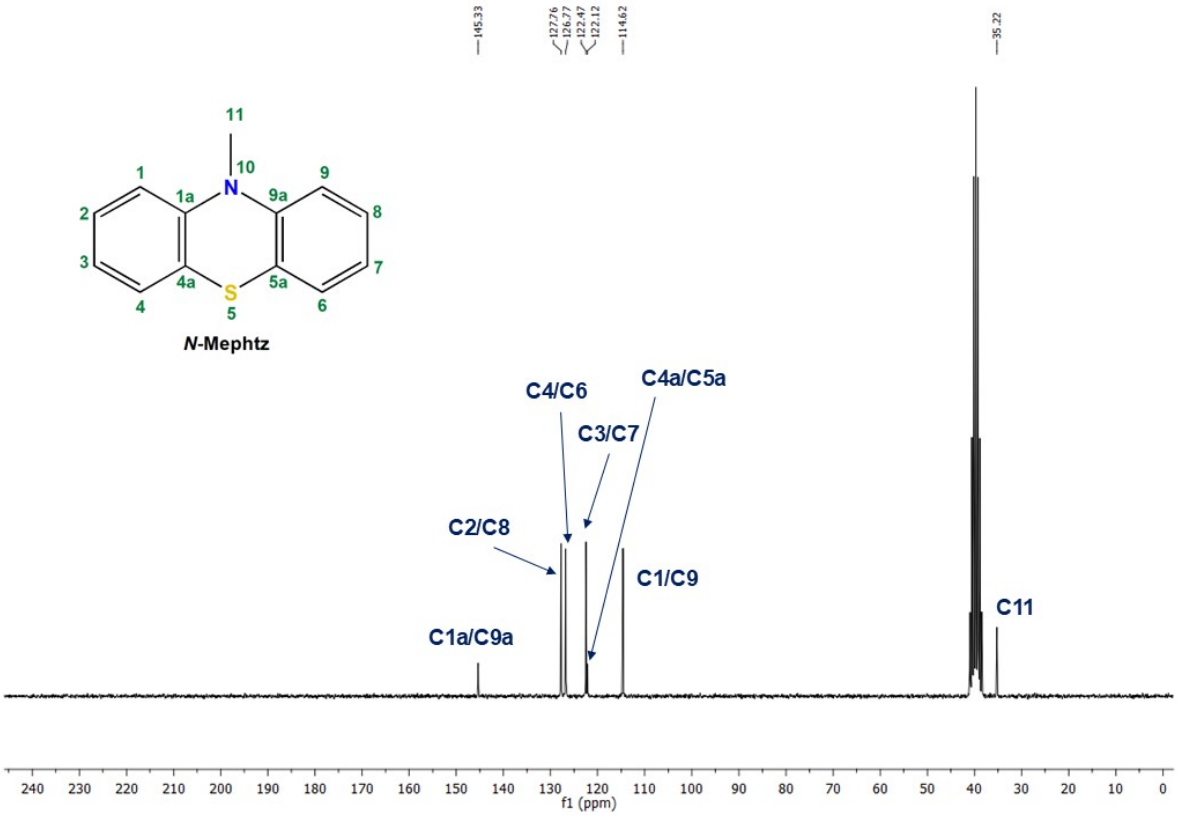

Fig. S3 ^{13}C NMR spectrum of *N*-Mephtz (DMSO-d_6, 50 MHz).

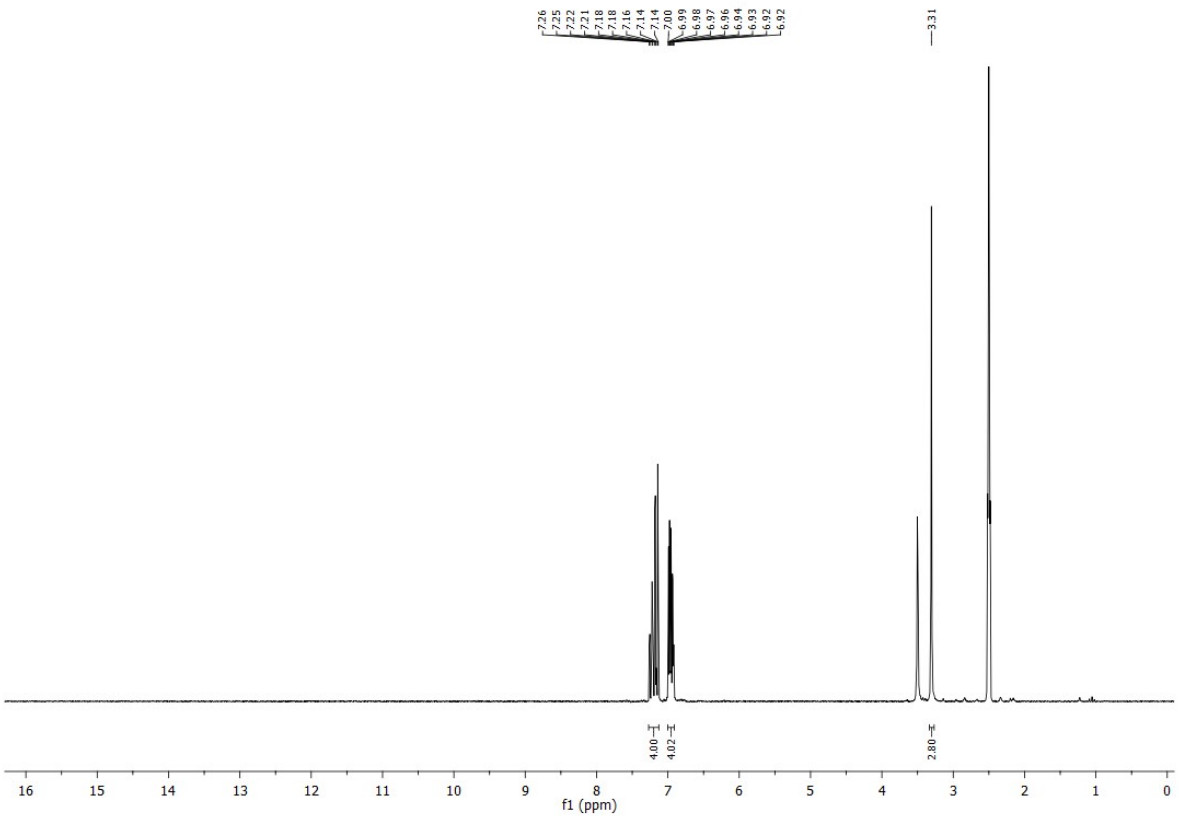

Fig. S4 ^{1}H NMR spectrum of complex **1** (DMSO-d_6, 200 MHz).

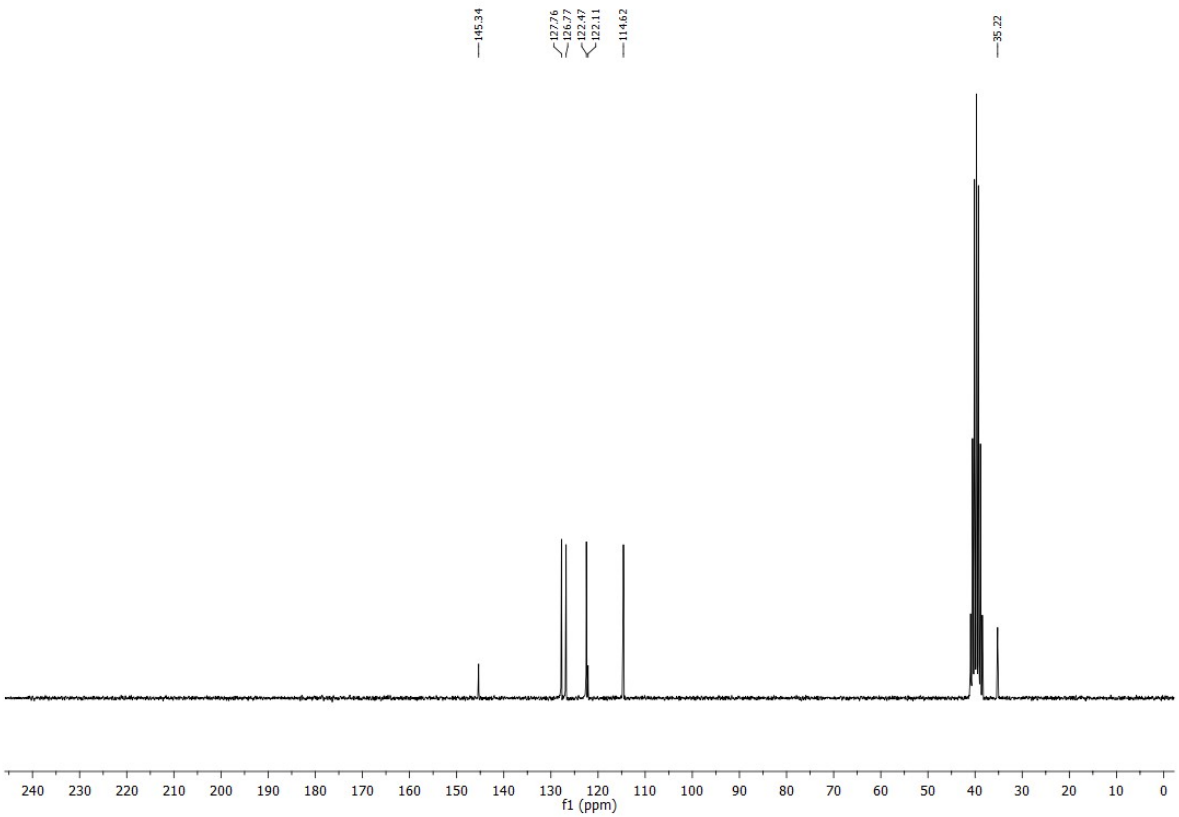

Fig. S5 ^{13}C NMR spectrum of complex **1** (DMSO-d_6, 50 MHz).

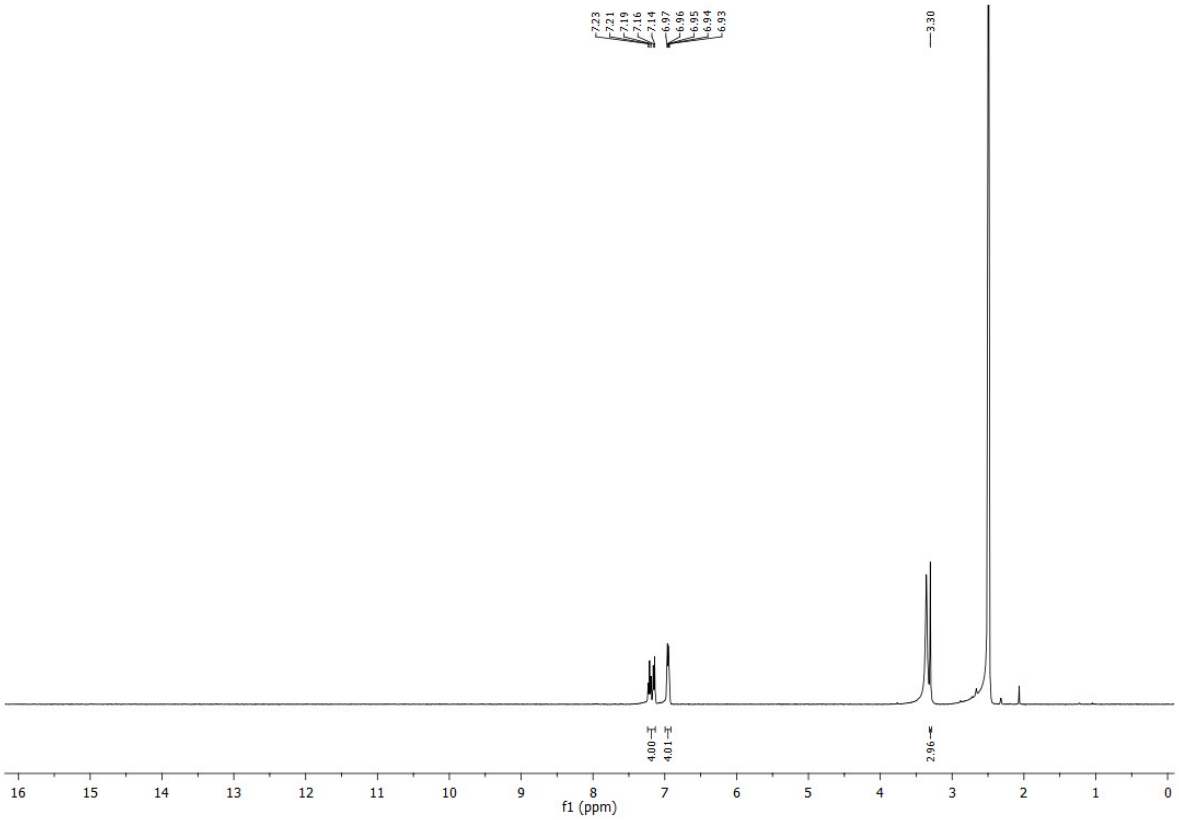

Fig. S6 ^{1}H NMR spectrum of complex **2** (DMSO-d_6, 200 MHz).

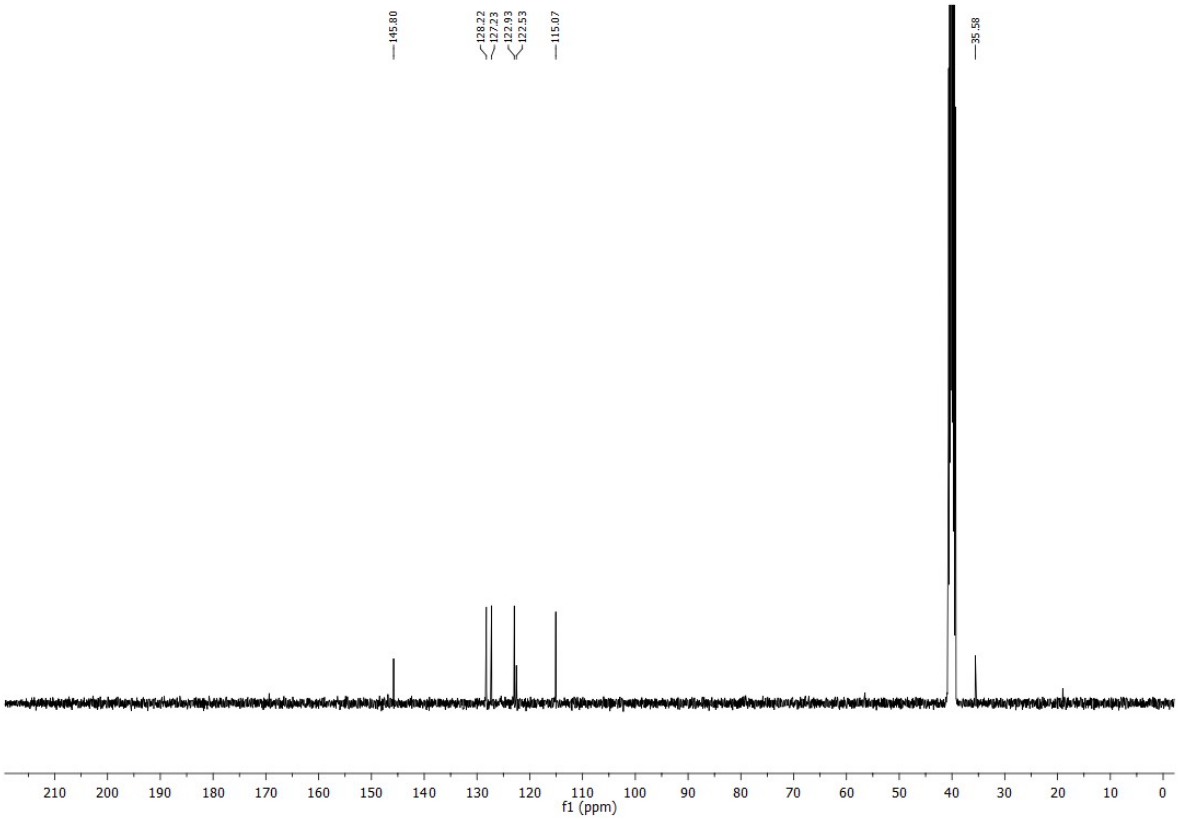

Fig. S7 ^{13}C NMR spectrum of complex **2** (DMSO-d_6, 50 MHz).

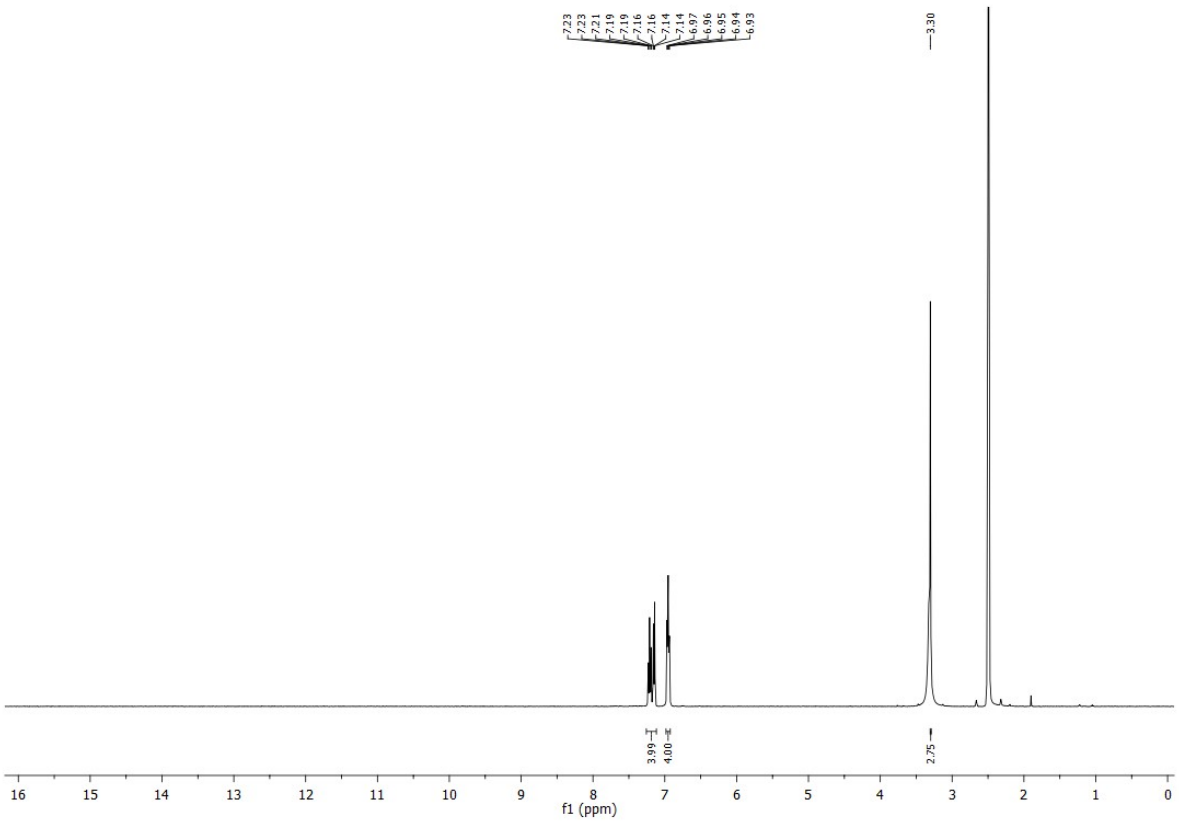

Fig. S8 ^{1}H NMR spectrum of complex **3** (DMSO-d_6, 200 MHz).

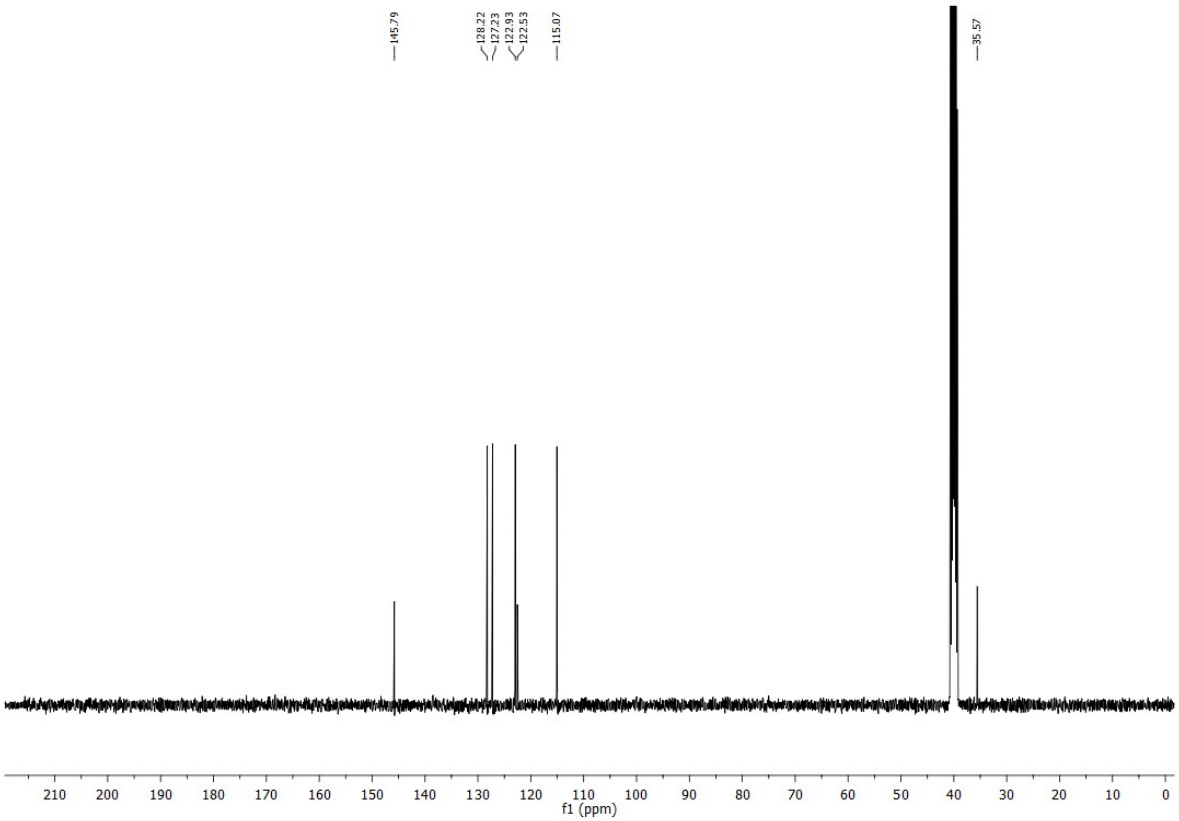

Fig. S9 ^{13}C NMR spectrum of complex **3** (DMSO-d_6, 50 MHz).

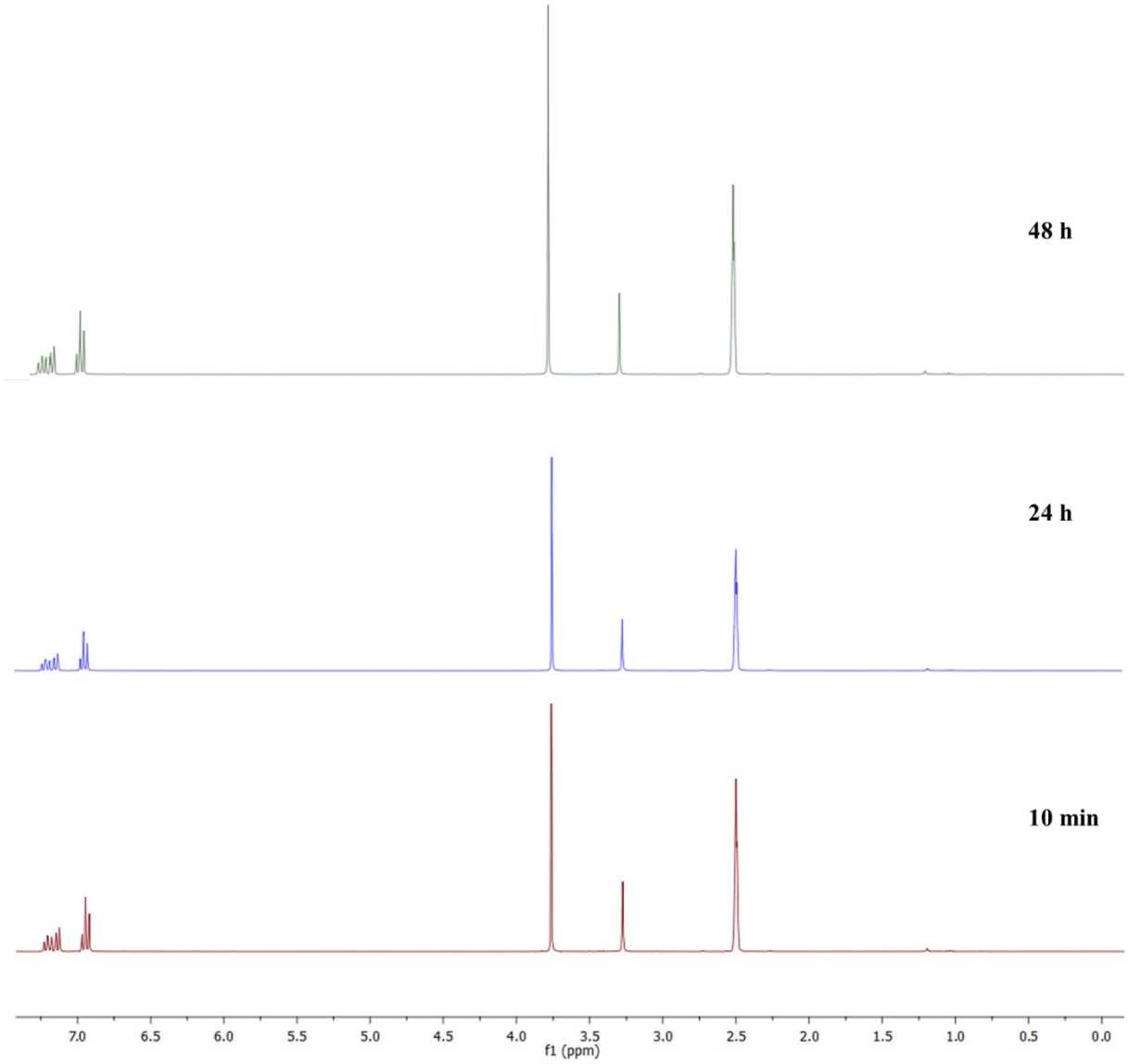

Fig. S10 ^{1}H NMR spectra of complex **3** recorded immediately, 24 h and 48 h after dissolving in DMSO-d_6/D_2O (v/v 9:1) at room temperature.

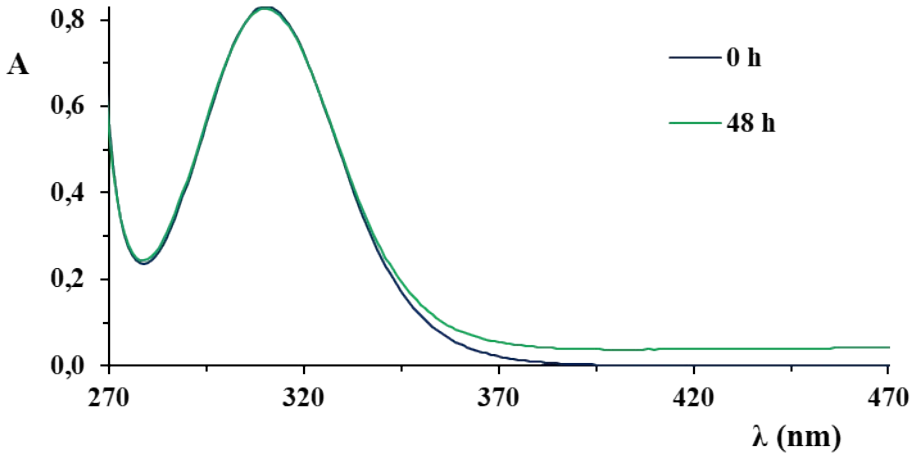

Fig. S11 UV-Vis spectra of complex **1** recorded immediately and 48 h after dissolving in DMSO at room temperature.

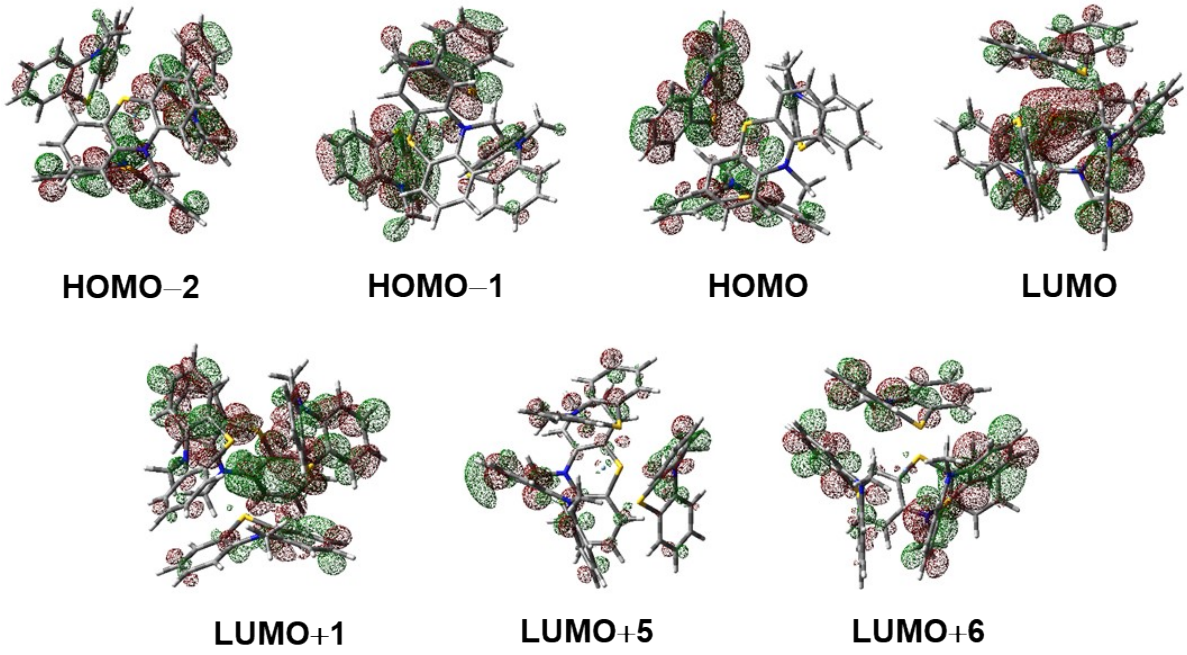

Fig. S12 Kohn-Sham orbitals of complex **1** (M06).

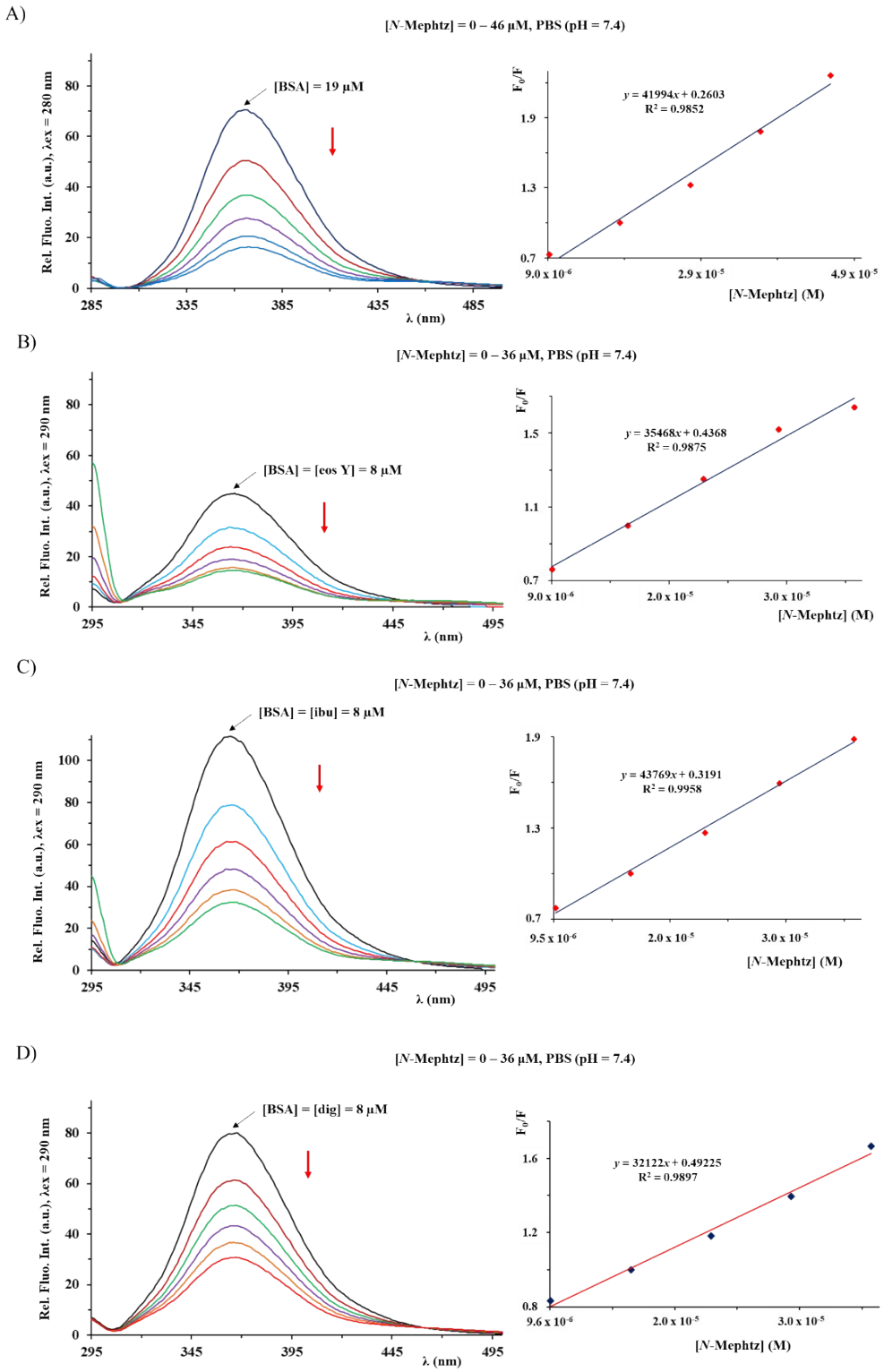

Fig. S13 The BSA emission spectra in the presence of an increasing concentration of *N*-Mephtz (A) and in presence of the site markers (B-D). The red arrow shows the changes of intensity after the addition of the compound. Inserted graph: Stern–Volmer plots of the F_0/F *vs.* [compound].

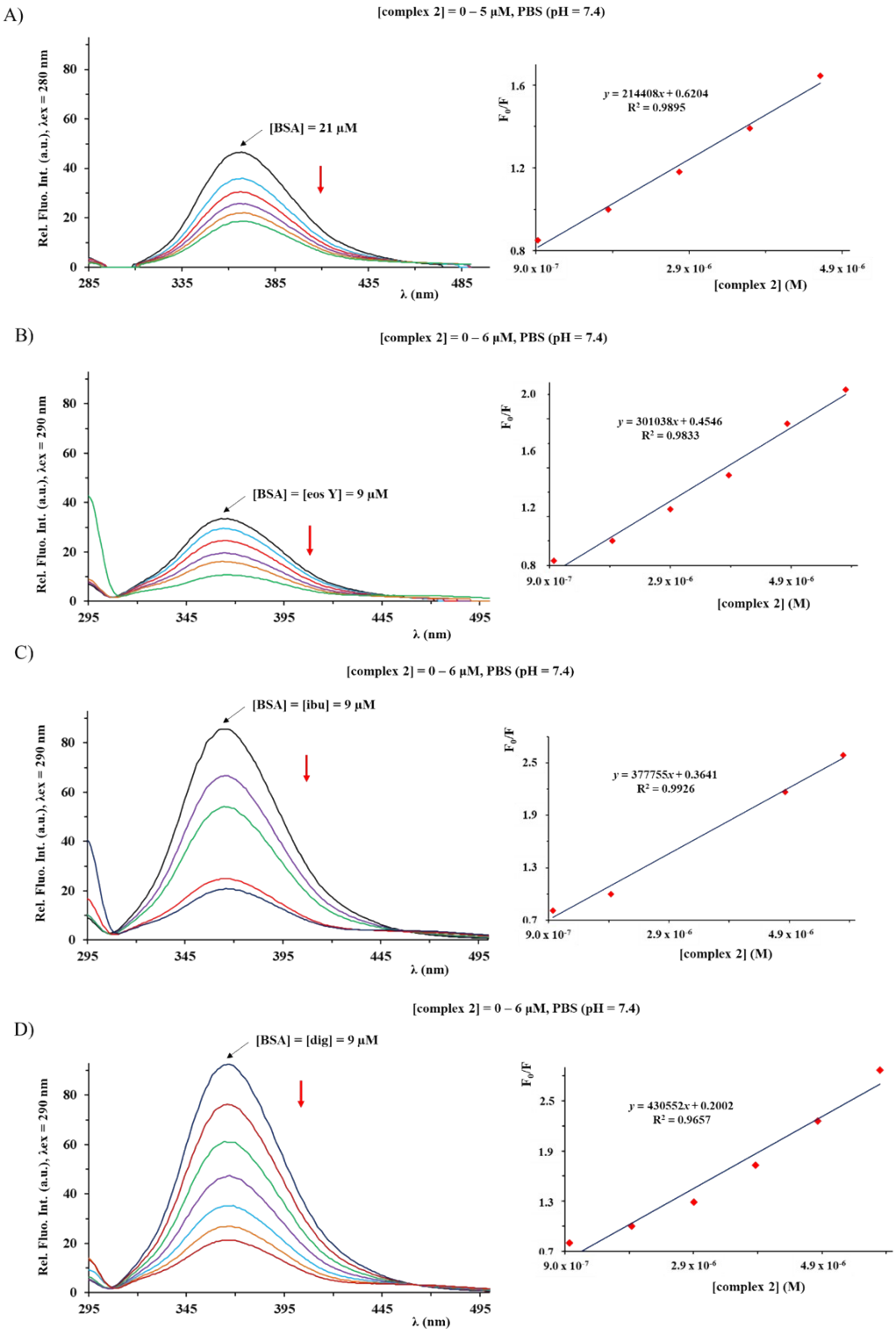

Fig. S14 The BSA emission spectra in the presence of an increasing concentration of complex **2** (A) and in presence of the site markers (B-D). The red arrow shows the changes of intensity after the addition of the compound. Inserted graph: Stern–Volmer plots of the F_0/F *vs.* [compound].

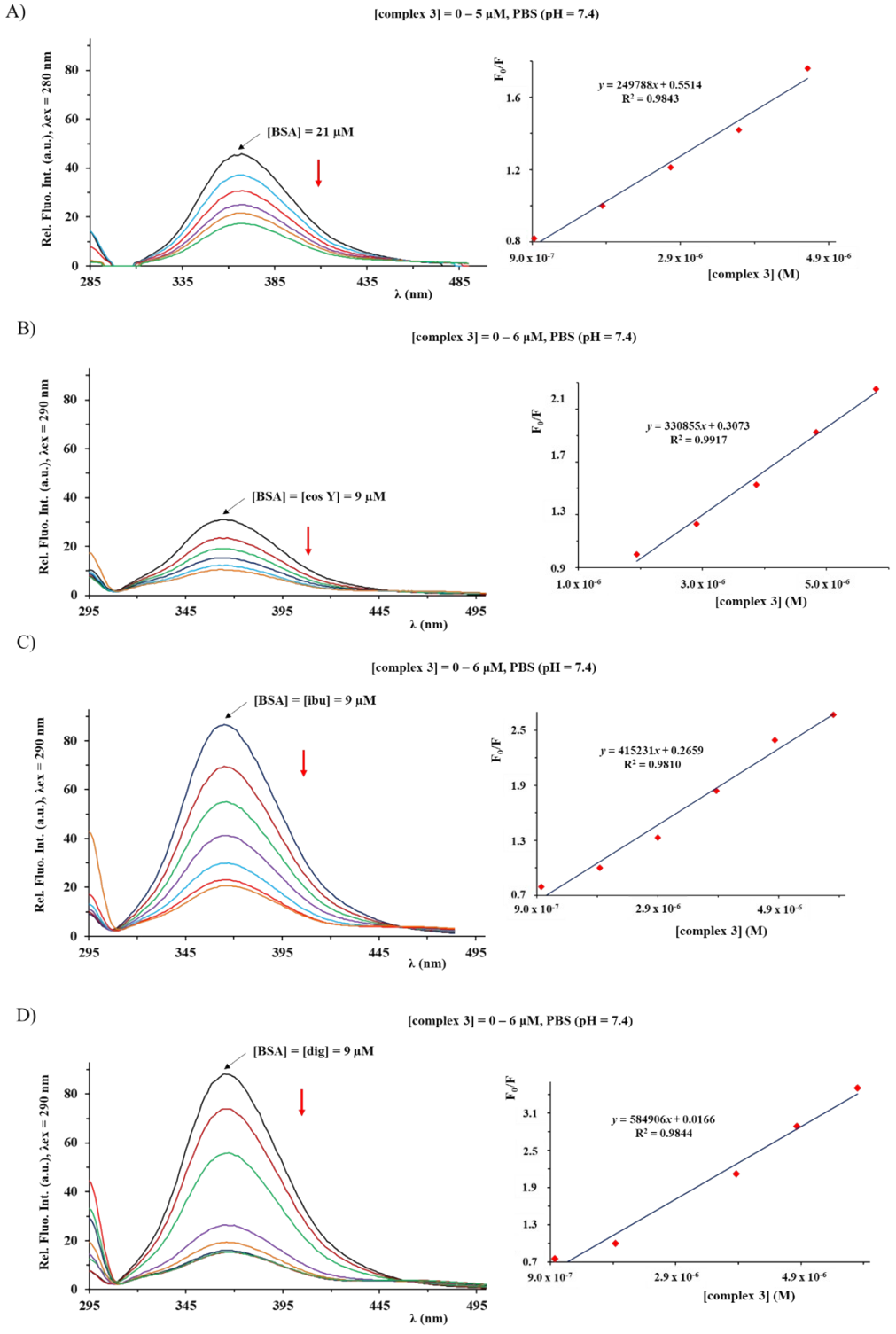

Fig. S15 The BSA emission spectra in the presence of an increasing concentration of complex **3** (A) and in presence of the site markers (B-D). The red arrow shows the changes of intensity after the addition of the complex. Inserted graph: Stern–Volmer plots of the F_0/F *vs.* [compound].

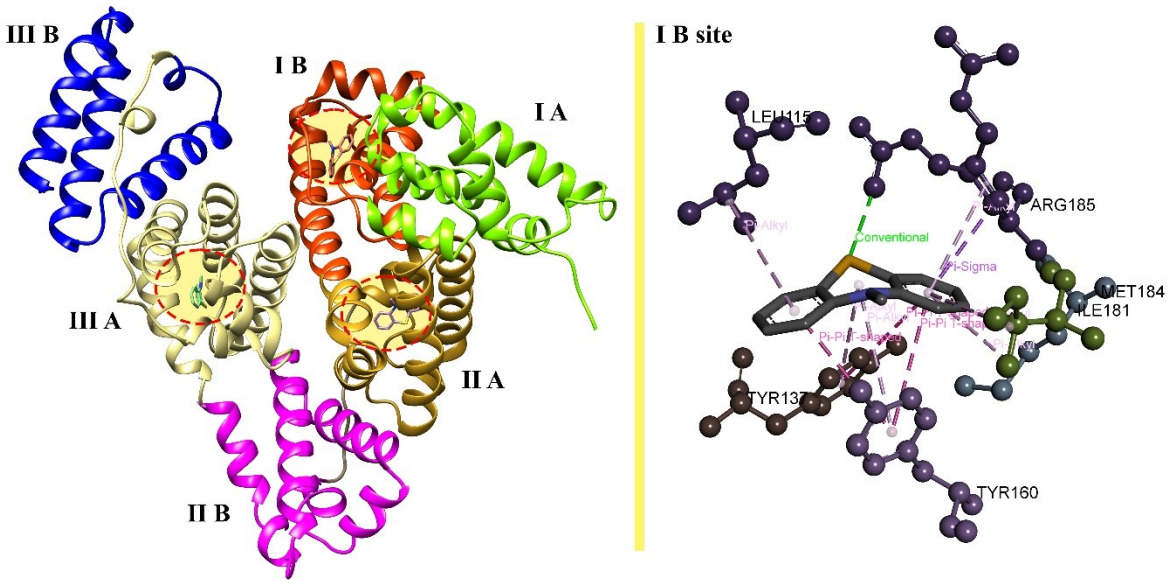

Fig. S16 The 3d superposition of the most favorable docking pose of *N*-Mephtz with BSA.

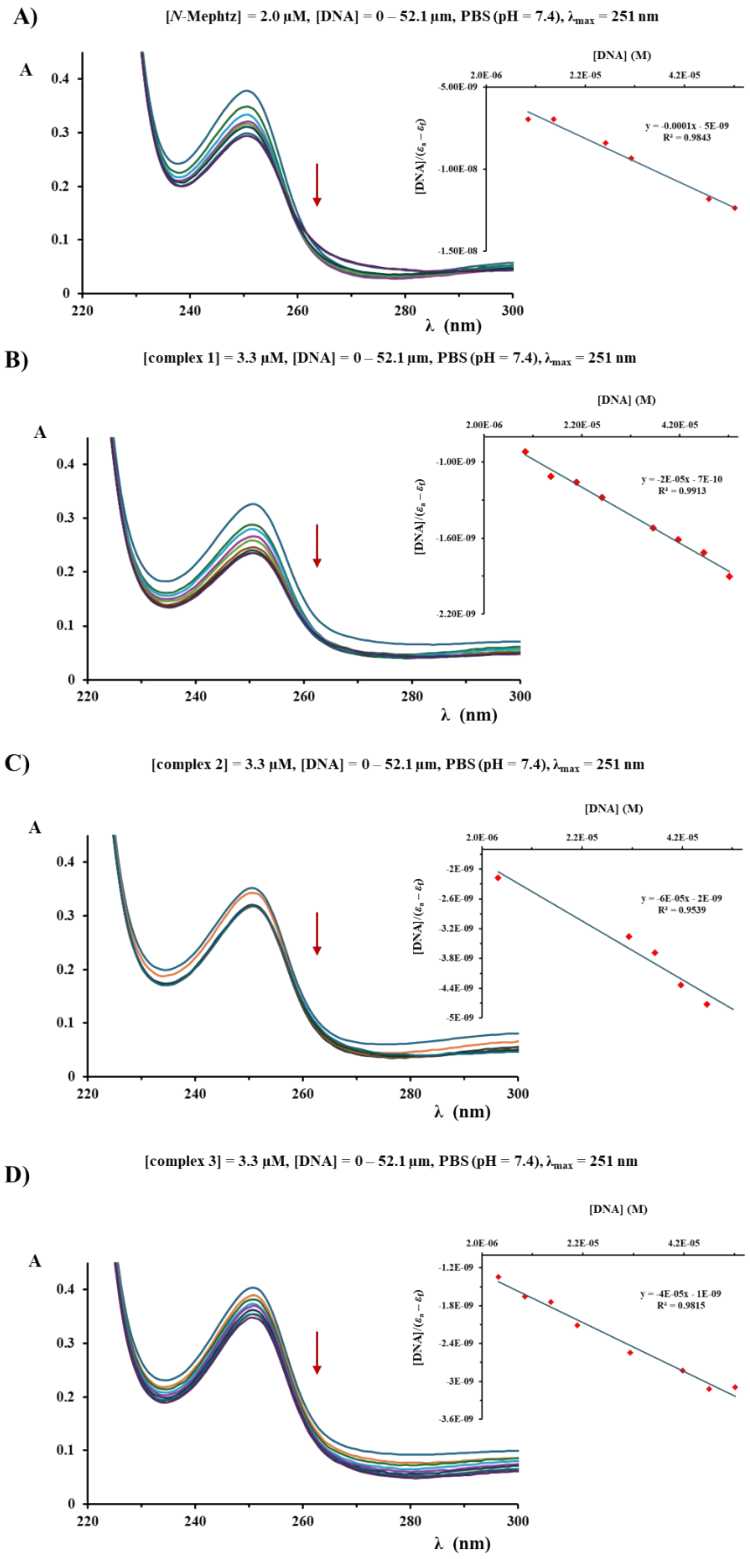

Fig. S17 UV-Vis absorption spectra of *N*-Mephtz (A) and silver(I) complexes (B – D) in the absence ($A_{complex}$) and presence ($A_{corr} = A_{complex+DNA} - A_{DNA}$) of ct-DNA. Arrow shows the change of absorbance upon increasing concentration of DNA. Inserted graph: Plot of [DNA]/($\varepsilon_a - \varepsilon_f$) *vs.* [DNA].

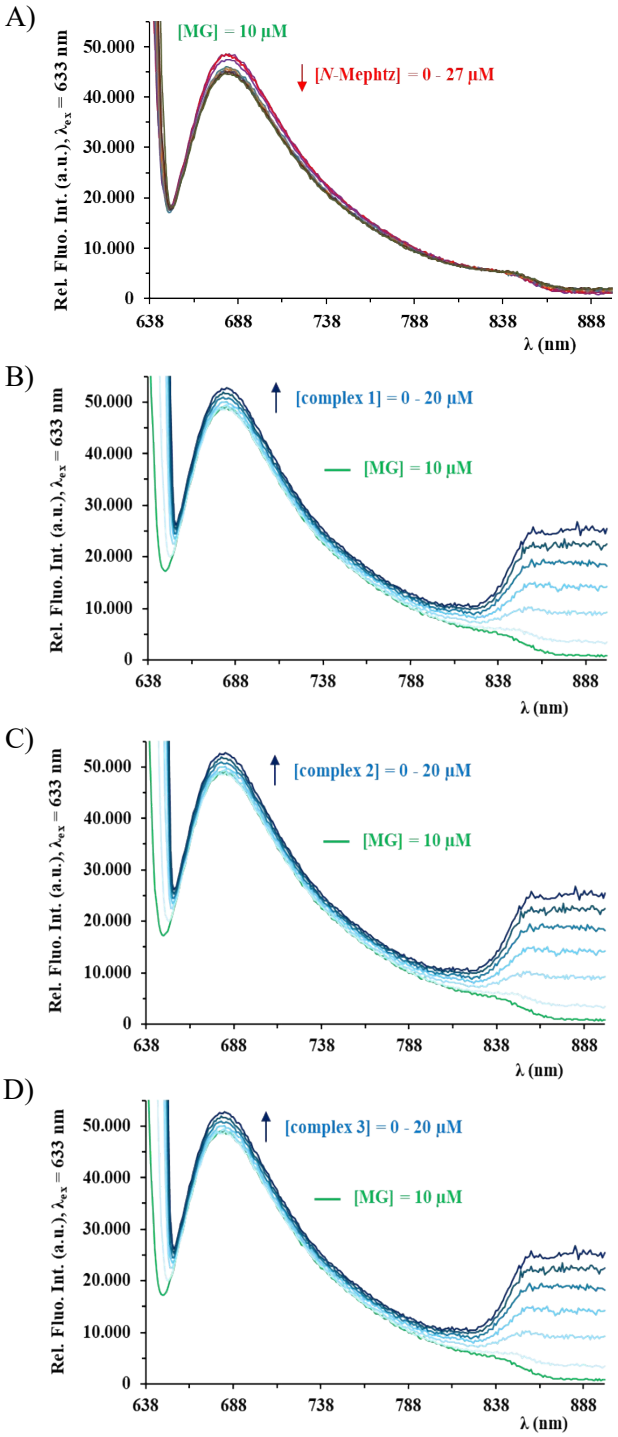

Fig. S18 Fluorescence emission spectra for the ct-DNA-MG system in PBS buffer in the presence of increasing amounts of *N*-Mephtz (A), and complexes **1–3** (B-D). The arrow shows the intensity changes upon increasing the concentration of the compound. Inserted graph: Stern–Volmer plots of the F_0/F *vs*. [compound].

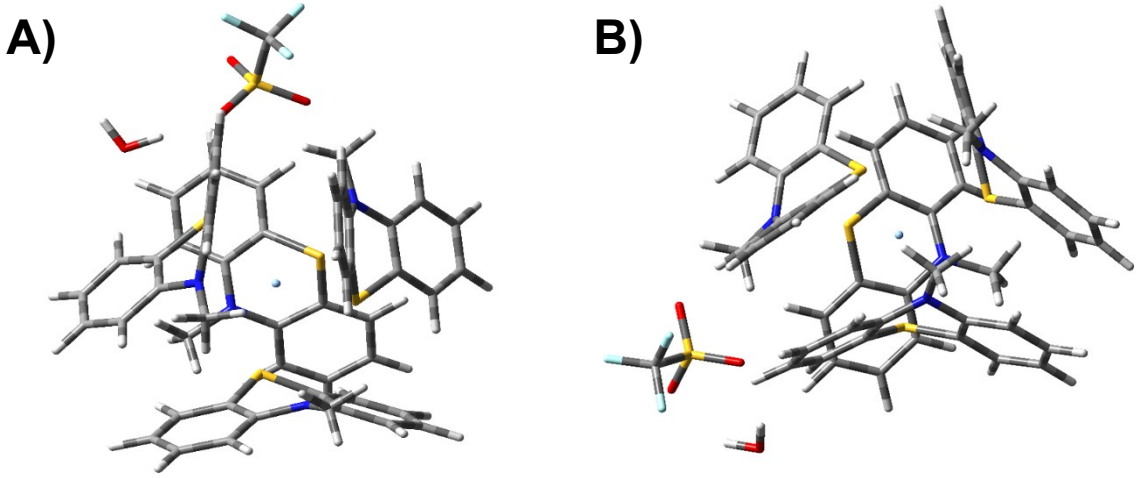

Fig. S19 Optimized geometries of complex **1** in the gas phase: A) B3LYP; B) M06.

Table S1 Selected bond lengths and angles in the crystal structures of complexes **1**–**3**.

Complex	**1**	**2**	**3**
Ag1-S1A	2.5939(8)	2.7425(8)	2.7511(8)
Ag1-S1B	2.57(1)	2.671(1)	2.6753(8)
Ag1-S1C	2.7999(9)	2.5138(8)	2.5056(7)
Ag1-S1D	2.5314(6)	2.5700(9)	2.5632(8)
S1A–Ag1–S1B	104.6(3)	93.80(3)	93.96(2)
S1A–Ag1–S1C	98.90(2)	107.50(3)	105.34(3)
S1A–Ag1–S1D	113.16(2)	100.87(3)	101.13(3)
S1B–Ag1–S1C	106.4(3)	115.12(3)	113.22(3)
S1B–Ag1–S1D	133.1(3)	99.63(3)	99.48(3)
S1C–Ag1–S1D	94.54(2)	132.62(3)	135.70(3)

Table S2 Comparison of experimental and calculated IR data for complex **1**.

	ν, cm^{-1}		
IR bands	Experimental	B3LYP	M06
ν(O–H)	3499, 3436	3689, 3428	3634, 3566
$\nu(C_{ar}–H)$	3147, 3060, 3010	3036, 3025	2985, 2948
ν(C–H)	2990, 2963	2975, 2936	2918, 2884
$\nu(C_{ar}=C_{ar})$	1595, 1573, 1459	1561, 1536, 1448	1555, 1529, 1429
$\nu_{as}(SO_3)$	1258	1180	1176
$\nu_{s}(CF_3)$	1223	1134	1154
$\nu_{as}(CF_3)$	1138	1064	1132
$\nu_{s}(SO_3)$	1031	928	964
$\gamma(C_{ar}–H)$	757	731	713

Table S3 Proteins used for molecular docking analysis.

Species	PDB(ref)	Protein	Role
E. coli			
	1hnj[1]	β-ketoacyl-acp synthase III	fatty acid biosynthesis
	1c14[2]	enoyl reductase	fatty acid biosynthesis
	5bnm[3]	FabH (β-ketoacyl-acyl carrier protein synthase III	fatty acid biosynthesis
	4hbt[4]	beta-lactamase	antibiotic resistance
	6f86[5]	DNA GyraseB	replication/transcription
	3t88[6]	1,4-dihydroxy-2-naphthoyl-CoA synthase –MenB	menaquinone biosynthesis
	6ntw[7]	transpeptidase YcbB	peptidoglycan cross-linking
S. aureus			
	2zco[8]	C(30) carotenoid dehydrosqualene synthase	cholesterol biosynthesis
	2xct[9]	DNA Gyrase	replication/transcription
	3u2d[10]	DNA gyrase subunit B	DNA synthesis
	1mwu[11]	Penicillin-binding protein 2a	cell wall synthesis
	5tw8[12]	Penicillin-binding protein 4	cell wall biosynthesis
	2w9s[13]	Dihydrofolate reductase	key metabolite biosynthesis
	1jij[14]	Tyrosyl-tRNA synthetase	protein synthesis
	4h8e[15]	Undecaprenyl pyrophosphate synthase	isoprenoid biosynthesis
P. aeruginosa			
	1u1z[16]	(3R)-hydroxyacyl-ACP dehydratase (FabZ)	fatty acid biosynthesis
	2uv0[17]	LasR ligand-binding domain	quorum-sensing
	3pbr[18]	Penicillin-binding protein PBP3	peptidoglycan synthesis
	3uwk[19]	Thymidylate kinase	thymidine triphosphate synthesis
	4b0c[20]	3-hydroxydecanoyl- ACP dehydratase (FabA)	fatty acid biosynthesis
	7m1m[21]	caseinolytic protease (Clp)	cellular physiology and stress responses
	7m1l[21]	caseinolytic protease (Clp)	cellular physiology and stress responses
	5oe3[22]	N-terminal domain of PqsA	quorum-sensing
C. albicans			
	5fsa[23]	sterol 14-alpha demethylase (CYP51)	sterol biosynthesis

References

[1] X. Qiu, C. A. Janson, W. W. Smith, M. Head, J. Lonsdale and A. K. Konstantinidis, *J. Mol. Biol.,* 2001, **307**, 341-356.

[2] X. Qiu, S. S. Abdel-Meguid, C. A. Janson, R. I. Court, M. G. Smyth and D. J. Payne, *Protein Sci.,* 2008, **8**, 2529-2532.

[3] D. C. McKinney, C. J. Eyermann, R.-F. Gu, J. Hu, S. L. Kazmirski, S. D. Lahiri, A. R. McKenzie, A. B. Shapiro and G. Breault, *ACS Infect. Dis.,* 2016, **2**, 456-464.

[4] S. D. Lahiri, S. Mangani, T. Durand-Reville, M. Benvenuti, F. De Luca, G. Sanyal and J.-D. Docquier, *Antimicrob. Agents Chemother.,* 2013, **57**, 2496-2505.

[5] S. Narramore, C. E. M. Stevenson, A. Maxwell, D. M. Lawson and C. W. G. Fishwick, *Bioorg. Med. Chem.,* 2019, **27**, 3546-3550.

[6] H.-J. Li, X. Li, N. Liu, H. Zhang, J. J. Truglio, S. Mishra, C. Kisker, M. Garcia-Diaz and P. J. Tonge, *Biochem.,* 2011, **50**, 9532-9544.

[7] N. A. Caveney, G. Caballero, H. Voedts, A. Niciforovic, L. J. Worrall, M. Vuckovic, M. Fonvielle, J.-E. Hugonnet, M. Arthur and N. C. J. Strynadka, *Nat. Commun.,* 2019, **10**, 1849.

[8] C.-I. Liu, G. Y. Liu, Y. Song, F. Yin, M. E. Hensler, W.-Y. Jeng, V. Nizet, A. H.-J. Wang and E. Oldfield, *Science,* 2008, **319**, 1391-1394.

[9] B. D. Bax, P. F. Chan, D. S. Eggleston, A. Fosberry, D. R. Gentry, F. Gorrec, I. Giordano, M. M. Hann, A. Hennessy, M. Hibbs, J. Huang, E. Jones, J. Jones, K. K. Brown, C. J. Lewis, E. W. May, M. R. Saunders, O. Singh, C. E. Spitzfaden, C. Shen, A. Shillings, A. J. Theobald, A. Wohlkonig, N. D. Pearson and M. N. Gwynn, *Nature,* 2010, **466**, 935-940.

[10] A. E. Eakin, O. Green, N. Hales, G. K. Walkup, S. Bist, A. Singh, G. Mullen, J. Bryant, K. Embrey, N. Gao, A. Breeze, D. Timms, B. Andrews, M. Uria-Nickelsen, J. Demeritt, J. T. Loch III, K. Hull, A. Blodgett, R. N. Illingworth, B. Prince, P. A. Boriack-Sjodin, S. Hauck, L. J. MacPherson, H. Ni and B. Sherer, *Antimicrob. Agents Chemother.,* 2012, **56**, 1240-1246.

[11] D. Lim and N. C. J. Strynadka, *Nat. Struct. Biol.,* 2002, **9**, 870-876.

[12] J. A. N. Alexander, S. S. Chatterjee, S. M. Hamilton, L. D. Eltis, H. F. Chambers and N. C. J. Strynadka, *J. Biol. Chem.,* 2018, **293**, 19854-19865.

[13] H. Heaslet, M. Harris, K. Fahnoe, R. Sarver, H. Putz, J. Chang, C. Subramanyam, G. Barreiro and J. R. Miller, *Proteins: Struct., Funct., Bioinf.,* 2009, **76**, 706-717.

[14] X. Qiu, C. A. Janson, W. W. Smith, S. M. Green, P. McDevitt, K. Johanson, P. Carter, M. Hibbs, C. Lewis, A. Chalker, A. Fosberry, J. Lalonde, J. Berge, P. Brown, C. S. V Houge-Frydrych and R. L. Jarvest, *Protein Sci.*, 2008, **10**, 2008-2016.

[15] W. Zhu, Y. Zhang, W. Sinko, M. E. Hensler, J. Olson, K. J. Molohon, S. Lindert, R. Cao, K. Li, K. Wang, Y. Wang, Y.-L. Liu, A. Sankovsky, C. A. F. de Oliveira, D. A. Mitchell, V. Nizet, J. A. McCammon and E. Oldfield, *Proc. Natl. Acad. Sci. U S A,* 2013, **110**, 123-128.

[16] M. S. Kimber, F. Martin, Y. Lu, S. Houston, M. Vedadi, A. Dharamsi, K. M. Fiebig, M. Schmid and C. O. Rock, *J. Biol. Chem.,* 2004, **279**, 52593-52602.

[17] M. J. Bottomley, E. Muraglia, R. Bazzo and A. Carfi, *J. Biol. Chem.,* 2007, **282**, 13592-13600.

[18] S. Han, R. P. Zaniewski, E. S. Marr, B. M. Lacey, A. P. Tomaras, A. Evdokimov, J. R. Miller and V. Shanmugasundaram, *Proc. Natl. Acad. Sci. U S A,* 2010, **107**, 22002-22007.

[19] J. Y. Choi, M. S. Plummer, J. Starr, C. R. Desbonnet, H. Soutter, J. Chang, J. R. Miller, K. Dillman, A. A. Miller and W. R. Roush, *J. Med. Chem.,*2012, **55**, 852-870.

[20] L. Moynié, S. M. Leckie, S. A. McMahon, F. G. Duthie, A. Koehnke, J. W. Taylor, M. S. Alphey, R. Brenk, A. D. Smith and J. H. Naismith, *J. Mol. Biol.,* 2013, **425**, 365-377.

[21] G. D. Mawla, B. M. Hall, G. Cárcamo-Oyarce, R. A. Grant, J. J. Zhang, J. R. Kardon, K. Ribbeck, R. T. Sauer and T. A. Baker, *Mol. Microbiol.,* 2021, **115**, 1094-1109.

[22] F. Witzgall, W. Ewert and W. Blankenfeldt, *ChemBioChem,* 2017, **18**, 2045-2055.

[23] T. Y. Hargrove, L. Friggeri, Z. Wawrzak, A. Qi, W. J. Hoekstra, R. J. Schotzinger, J. D. York, F. P. Guengerich and G. I. Lepesheva, *J. Biol. Chem.,* 2017, **292**, 6728-6743.

Table S4 Binding constants of the *N*-Mephtz ligand with ct-DNA-MG system.

compound	K_{sv} (M^{-1})	Hypochromism (%)	K_q ($M^{-1}s^{-1}$)	K_A (M^{-1})	*n*
N-Mephtz	(3.86 ± 0.04) x 10^3	9.1	3.86 x 10^{11}	1.52 x 10^4	1.13

Table S5 Crystallographic data for silver(I) complexes **1–3**.

	1	**2**	**3**
Crystal data			
Chemical formula	$C_{52}H_{44}AgN_4S_4 \cdot CF_3O_3S \cdot 0.333H_2O$	$C_{52}H_{44}AgN_4S_4 \cdot F_6Sb$	$C_{52}H_{44}AgN_4S_4 \cdot F_6P$
M_r	1116.09	1196.77	1105.99
Crystal system	Triclinic	Orthorhombic	Orthorhombic
Space group	$P\bar{1}$	*Pbca*	*Pbca*
Temperature, K	296	295	295
a / Å	12.1078(2)	14.3577(2)	14.1327(2)
b / Å	12.8639(2)	22.6188(3)	22.4083(4)
c / Å	16.6110(4)	30.3788(5)	30.6416(5)
α / °	78.6520(17)	90	90
β / °	76.3114(17)	90	90
γ / °	87.9851(14)	90	90
V / Å^3	2464.41(9)	9865.6(3)	9703.9(3)
Z	2	8	8
μ / mm^{-1}	0.68	1.18	0.69
Crystal size, mm	0.86 × 0.62 × 0.18	0.90 × 0.63 × 0.43	0.64 × 0.51 × 0.38
Data collection			
Diffractometer	Gemini S (Oxford Diffraction)	Gemini S (Oxford Diffraction)	Gemini S (Oxford Diffraction)
Absorption correction	Multi-scan	Multi-scan	Multi-scan
T_{min}	0.863	0.837	0.866
T_{max}	1.000	1.000	1.000
No. of measured reflections	103061	65568	42730
No. of independent reflections	10084	10089	9915
No.of observed [$I > 2\sigma(I)$] reflections	8510	8276	7825
R_{int}	0.037	0.030	0.029
$(\sin \theta/\lambda)_{max}$ / Å^{-1}	0.625	0.625	0.625
Refinement			
$R[F^2 > 2\sigma(F^2)]$	0.039	0.035	0.036
$wR(F^2)$	0.106	0.092	0.093
S	1.01	1.01	1.02
No. of reflections	10084	10089	9915
No. of parameters	731	618	673
No. of restraints	14	0	448
H-atom treatment	Mixed	Constrained	Constrained
$\Delta\rho_{max}$ / e Å^{-3}	1.00	0.76	0.63
$\Delta\rho_{min}$ / e Å^{-3}	−0.61	−0.67	−0.63

Table S6 Grid box parameters (spacing 0.375) used in molecular docking with selected targets. Blind docking was performed in the case of 1u1z and 4b0c.

PDB ID	center (x, y, z)	size (x, y, z)
1hnj	1) 27, 14,9, 31.1 2) 42.5, 27.5, 24	1) 77, 82, 61 2) 66, 61, 56
3t88	-34, 7.2, -23	72, 72, 72
1jij	-12.4, 19.5, 80.6	114, 85, 98
1u1z	19.1, 41.7, 126.8	96, 85, 90
2uv0	26, 10.9, 77.4	112, 125, 152
4b0c	24.9, -13.3, 23	58, 58, 58
7m1l	20.3, 50.8, 31.7	149, 125, 146
5fsa	191.2, 7.2, 40.5	72, 98, 69
4f5s	8.8, 24.8, 103	264, 240, 258
1bna	14.8, 21.5, 9.3	106, 106, 133